Earth and Planetary Science Letters 295 (2010) 187–194

Contents lists available at ScienceDirect

Earth and Planetary Science Letters

journal homepage: www.elsevier.com/locate/epsl

Tectonic and dynamic controls on the topography and subsidence of the Argentine Pampas: The role of the flat slab

Federico M. Dávila [a,*], Carolina Lithgow-Bertelloni [b], Mario Giménez [c]

[a] Centro de Análisis de Cuencas, CICTERRA-CONICET, Universidad Nacional de Córdoba, Av. Vélez Sársfield 1611, X5016GCA Córdoba, Argentina
[b] Department of Earth Sciences, University College London, Gower St., London WC1E 6BT, UK
[c] Instituto Geofísico Sismológico Volponi, Facultad de Ciencias Exactas, Físicas y Naturales. Universidad Nacional de San Juan, Meglioli 1160-S. CP: 5400, Rivadavia, San Juan, Argentina

ARTICLE INFO

Article history:
Received 19 October 2009
Received in revised form 15 March 2010
Accepted 25 March 2010
Available online 28 April 2010

Editor: Y. Ricard

Keywords:
basin analysis
dynamic topography
flat subduction
Andean foreland
Argentina
Pampas Plain

ABSTRACT

We analyze the Pampean foreland (the Pampas) along the modern flat-slab segment of the south-central Andes between 31° and 33° South latitude and to the east of the Argentine "flat-slab" province, using flexural and gravity studies and computations of dynamic topography. Bouguer anomalies and flexural analysis predict a foredeep of ~250 km width and a peripheral bulge amplitude of ~25 m, which match the regional morphologies of the modern Argentine Pampean Plain. However, these studies do not account for the subsurface Miocene–Quaternary basin preservation, represented by sedimentary thicknesses >400 m and with depocenters >400 km eastward with respect to flexural models. The discrepancy suggests that two mechanisms, acting at different wavelengths, influence the Argentine Pampas. The basin preservation is likely the result of a large-scale geodynamic forcing. Models of mantle flow, driven by realistic flat-slab subduction geometry and density contrasts, reproduce the depocenter location and the wavelength of subsidence as well as most of the remaining amplitude. Nonetheless, more sophisticated studies (e.g. considering lateral viscosity variations in the mantle wedge) might help reduce the dynamic amplitudes and better reproduce the observed geological record.

1. Introduction

Tectonic topography driven by crustal shortening is often considered the main control for bending and flexure of the lithosphere. It is this flexure, which is responsible for generating the accommodation space necessary for foreland basin systems (DeCelles and Giles, 1996). In the Central Andes we find one of the most outstanding natural analogues of foreland systems between the high plateau of Bolivia and the lowlands of Brazil, at ~16°–20° South latitude (see Horton and DeCelles, 1997). Further south between 31° and 33° South latitude, along the modern Pampean flat-slab segment, the foreland basin system model has not been examined. Studies have only focused on the more proximal depocenters, close to the fold-and-thrust belt (Jordan et al., 1993). The occurrence of east and west vergent, deep-angle, crystalline-basement thrusts, which fragment the foreland plains (Fig. 1), complicates the simple picture, for example in the preservation of deep 'broken foreland' basins (Dávila et al., 2007). Cratonward, eastward from the Argentina broken foreland, the Pampean plain records hundreds of meters of Miocene deposits in the subsurface (Marengo, 2006; Fig. 1B, C). Although this record has been broadly classified as a foreland (Chebli et al., 1999), the subsidence mechanisms are still not well understood. DeCelles and Giles (1996) briefly discussed the possibility of sub-crustal loading in the Andes, while focusing largely on supracrustal loads and flexure. However, Dávila et al. (2007) proposed that non-isostatic loads, related to mantle dynamics (dynamic topography), played an important role in the configuration of the pericratonic foreland basins in South America, especially in this region where flat subduction is presently active, similar to the hypotheses for the formation of the early Cenozoic Laramide basins in the Western Interior, United States (e.g. Mitrovica et al., 1989; Liu and Nummedal, 2004). Flat subduction is traditionally associated with large episodes of dynamic subsidence (e.g. Liu et al., 2008). Mantle flow induces radial stresses, which deflect the surface and directly connect Earth's interior processes with crustal deformation and basin formation (e.g., Pysklywec and Mitrovica, 1999). Elucidating this connection and constraining these processes from long to short wavelengths are central to gain a better understanding of the connection between mantle dynamics and surface subsidence and uplift. The flat slab segment of the Central Andes in Argentina is an ideal location because the slab geometry is well known from Miocene times (Kay and Mpodozis, 2002) and the foreland basins are superbly preserved. We conducted an integrated basin analysis along the Andean foreland at ~31° South latitude between the easternmost basement highs of the broken foreland and the Argentine plain (~65°–63° West longitude) (Fig. 1B), combining flexural modeling with geomorphologic, stratigraphic and

* Corresponding author.
E-mail address: fmdavila@efn.uncor.edu (F.M. Dávila).

0012-821X/$ – see front matter © 2010 Elsevier B.V. All rights reserved.
doi:10.1016/j.epsl.2010.03.039

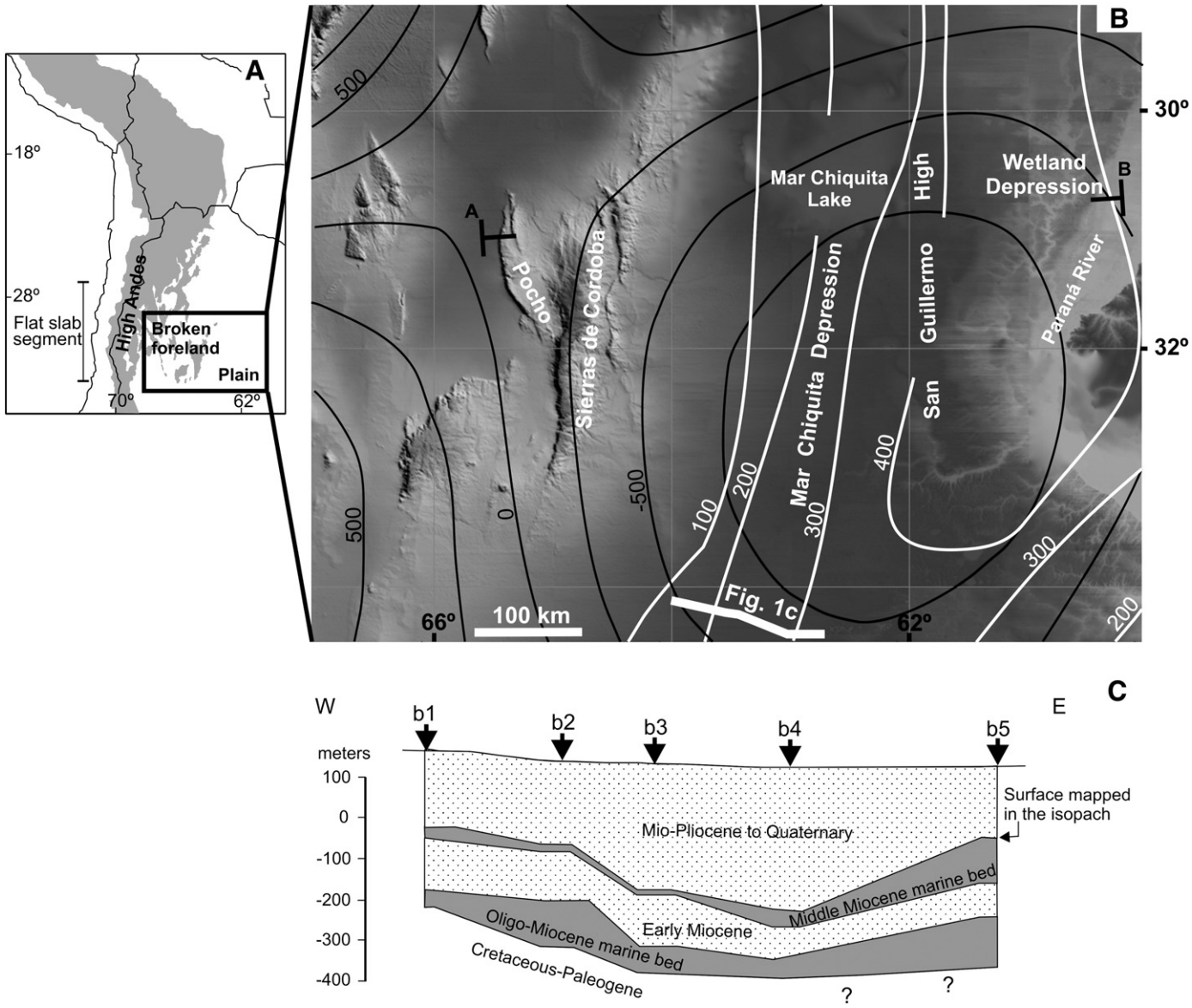

Fig. 1. (A) Study area within the S-Central Andes and location of the broken foreland and Pampas to >900 km from the trench. (B) Digital elevation model of the modern Argentine foreland depicting the major morphological units. White lines are isopachs (meters), embracing deposits from Mio–Pliocene to Present, and black lines are dynamic topography (meters) calculated in this work. The morphological profile A–B is shown in Fig. 2. (C) Stratigraphic cross-section (after Marengo, 2006). Location of the section is shown in the bottom of Fig. 1(B). The gray layers are marine beds, whereas the dot-pattern strata are alluvial successions. b1, b2, b3, b4 and b5 are boreholes.

geophysical studies along with mantle flow calculations of dynamic topography.

2. Tectonic setting, geology and geomorphology

Between 31° and 33° South latitude, to >500 km eastward from the high Cordillera, the Central Andes is represented by a geological province analogous to the Laramide orogeny in the western US, where crystalline basement is involved in deformation (Jordan and Allmendinger, 1986). This province is known as the Sierras Pampeanas broken foreland and is formed mainly by Proterozoic to Paleozoic basement ranges. The easternmost range is the Sierras de Cordoba, bounded to the east by the Argentine plain, also known as the Pampean Plain or the Pampas (Fig. 1). A recent subsurface stratigraphic compilation and analysis (Marengo, 2006) allowed us to reconstruct the Miocene–modern thicknesses in the Pampean plain (Fig. 1B, C) sedimentary interval analyzed in this work. The stratigraphy was based on >200 data from boreholes, with ages constrained by micropaleontology, and assisted by correlation using hundreds of kilometers of industry reflection seismic sections. The borehole data was limited horizontally to the section shown in Fig. 1C, although we use existing maps and seismic sections (Marengo, 2006) across the entire foreland to put limit on the isopach map we show in Fig. 1B.

The Cenozoic of the Pampas subsurface overlies Proterozoic to Mesozoic units (Chebli et al., 1999; Ramos, 2008), and is composed of ≤500-m thick Oligo–Miocene (Laguna Paiva Fm) to Neogene (Chaco and Paraná Fms) units (Marengo, 2006) (Fig. 1C). These are essentially alluvial sequences interfingered by two shallow marine horizons (Oligo–Miocene and Middle Miocene, cf. Marengo, 2006). But only the middle Miocene marker (Paranaense incursion bed, see also Hernández et al., 2005) has a particular interest for our analysis because it constrains the tectonic loading and flexural history of the Pampas, when the Sierras de Cordoba rose (<7 Ma, see below).

Between the Sierras de Cordoba and the Paleo–Proterozoic cratonic areas, located to the east, five morphostructural regions develop (Figs. 1B and 2): (1) the Sierras de Cordoba basement-thrusting belt, with elevations between ~3000 and ~1000 m above

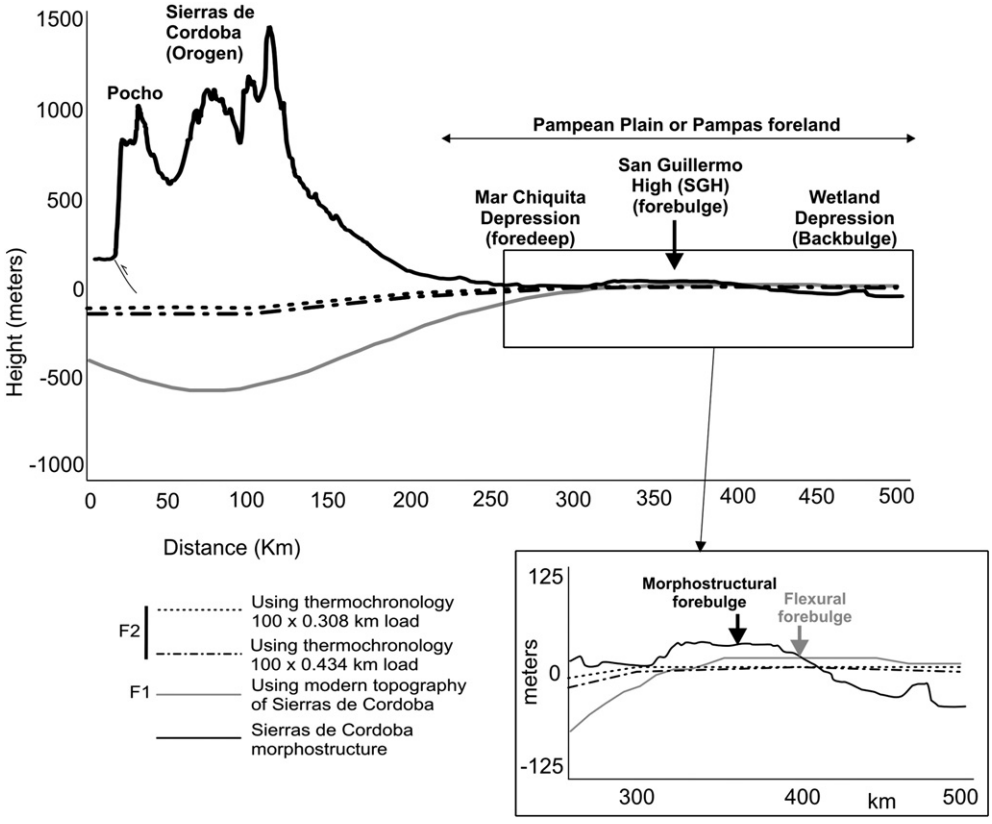

Fig. 2. Topography/morphostructure (location in Fig. 1B, profile A–B) and flexural models between the Sierras de Cordoba and the Pampas foreland using the modern relief (gray line, F1) and a thermochronologic approach (dash lines, F2). The inset depicts details in the forebulge zone and compares the location of the modeled (flexural) and observed (morphostructural) bulges.

sea level; (2) an extended alluvial bajada, formed by megafans; (3) the Mar Chiquita lake depression, limited to the east by (4) a low-relief topography (30–40 m high), known as the San Guillermo High; and (5) a wetland area, to the east of San Guillermo High, that hosts a set of lagoons that make up a large and long depression (>90,000 km^2). Regions (3), (4) and (5) comprise the Argentine Pampas. The distance between the mountain system and the San Guillermo High is ~230 km (Fig. 2). Brunetto (2008) interpreted two subsurface normal faults, involving Tertiary sequences, bounding the east and west flanks of the San Guillermo High (Fig. 2), inverted during regional compression and draped by Quaternary loess. No record of historical and active crustal seismicity has been described in the Pampas.

3. Methodology

3.1. Flexural analysis

The lithospheric bending triggered by the Sierras de Cordoba topography was computed using the 2D formulation of Cardozo and Jordan (2001) (see Appendix A). The density values of the loads used here are: ∂_b 2700 kg/m^3, where basement rocks dominate, and ∂_{sr} 2600 kg/m^3 in the foothills, where alluvial fans and Cenozoic rocks crop out. This model assumes flexural compensation with respect to the mantle ($\partial_m = 3300$ kg/m^3). Effective elastic thicknesses (Te) of 30 to 50 km were analyzed, consistent with recent geophysical approaches (Tassara, 2005; Tassara et al., 2007; Pérez-Gussinyé et al., 2007). Nevertheless, because this portion of the Argentine foreland was dominantly cratonic since the Cenozoic and that our central objective is not to fit isostatic flexural curves to the basin geometry by changing the rigidity, we used a homogeneous (in space and time) Te, consistent with the mean values of the modern plain, i.e. ~50 km (Pérez-Gussinyé et al., 2007). But in fact, this simplification has no significant implications on the flexural profiles given the small values of deformation recorded in this region (e.g., changes of 10–20 km in Te reproduce flexural curves only 20–30 meters apart). The influence of the compressive stress on distal foreland lithosphere was not evaluated because GPS intraplate velocity studies have demonstrated insignificant displacement in the Pampas (Brooks et al., 2003).

Our analysis focuses on a section spanning from the Sierras de Cordoba topography to the Pampas plain across the modern foreland by ~500 km. We estimated the maximum length of loads affecting our basin (MLB) using the model of Garcia-Castellanos et al. (2002), from which we can calculate the distance at which loads can contribute to the deflection of the basin. We limit our use of this model to the maximum distance at which the load affects basin subsidence and allows us to quickly test different load geometries. Calculations assume an infinite 1-D thin elastic plate with constant elastic thickness (Te), as detailed in Turcotte and Schubert (2002). Further extension to 2 and 3-D was beyond our present scope, but has been For Te between 40 and 50 km, the maximum load MLB is located at ~150–100 km. Since the distance from the Pampean Plain to the westernmost Sierras de Cordoba range (Pocho range, Fig. 1B) is ~120 km, and the next basement range to the west is located >200 km away, we only consider the Sierras de Cordoba as the main topographic load. Our model assumes the high Cordillera would have not exerted any contribution on the accommodation of the sedimentary systems of the Pampean Plain.

Two loading scenarios were tested (Appendix A): (1) assuming as load the entire modern topography of the Sierras de Cordoba (profile A–B in Figs. 1B and 2), referred as F1, and (2) estimating the Tertiary uplift, referred as F2, which better represents the true tectonic load. In scenario F1, the topographic profile from the westernmost to the easternmost part of the Sierras de Cordoba (Fig. 2) was re-drawn in

discrete rectangles, which represents the tectonic + sedimentary loads. In the scenario F2, the loading is a rectangle of length equal to the width of the Sierras de Cordoba, and height equal to the uplift estimated from available apatite fission track thermochronology (see below).

3.2. Bouguer anomalies

For this analysis we used a total of 1400 gravimetric values located between the Sierras de Cordoba and the Pampean Plain, obtained from the database of the Instituto Geofísico Sismológico Volponi, Universidad Nacional de San Juan, linked to the reference value in Miguelete (province of Buenos Aires) in the System IGSN1971.

We calculated gravity anomalies following Hinze et al. (2005). A normal gradient of −0.3086 mGal/m was used for the free air correction, and a density of 2.67 g/cm^3 for the Bouguer correction (Hinze, 2003). The gravimetric observations were reduced topographically via Hayford zones up to circular zones with a diameter of 167 km using the Digital Elevation Model obtained from the Shuttle Radar Topography Mission (SRTM) of the U.S. Geological Survey and NASA, combining the algorithms developed by Kane (1962) and Nagy (1966). Gravity grids were plotted using the minimum curvature method, which is usually sufficient to regularize field points measured at unevenly spaced stations on a topographic surface.

3.3. Dynamic topography

Deformation of Earth's surface driven by mantle flow (dynamic topography) can influence the accommodation space balance (Gurnis, 1990), supplementing the topographic loads. We calculate dynamic topography by solving for the radial stresses of the instantaneous viscous flow induced in the mantle by a given 3-D mass distribution. The equations of conservation of mass and momentum for a Newtonian viscous fluid, together with Poisson's equation for the gravitational potential are solved in a spherical shell via propagator matrices (Hager and O'Connell, 1981). The method allows for radial viscosity variations and the use of any density heterogeneity. We computed flow at harmonic degree and order 50 (~800 km wavelength). We took as a starting point a radial viscosity structure for the mantle and a global density heterogeneity model based on the accumulation of slab remnants transported into the mantle during subduction (Ricard et al., 1993) (Appendix A). In this model slabs are the only source of buoyancy. Slablets are dropped vertically at the trench and sink through the mantle with effective non-vertical dip angles arising from trench rollback (measured as the difference in trench position from tectonic stage to tectonic stage) and the viscosity contrast between upper and lower mantle. This approach has shown great success at reproducing the Earth's geoid and plate driving forces (Ricard et al., 1993; Lithgow-Bertelloni and Richards, 1998). Density contrasts between sinking slablets and mantle are modified by the age of the slab at the time of subduction and are as high as 72 kg/m^3. These simple kinematic slab models do not account for the dramatic variations in dip angle of the Nazca plate along strike, and predict vertical subduction along the margin rather than inland. To approximate this geographic disparity we migrated the slablets to ~64° West longitude (Fig. 3), where the flat slab submerges again below the easternmost flank of the Sierras de Cordoba (Booker et al., 2004). We examined the effects of a variety of viscosity structures on the amplitude of dynamic topography (Appendix A and Fig. 3), ranging from a lithosphere (L) whose viscosity is equal to that of the upper mantle (UM) to one 1000 times more viscous and a lower mantle (LM) 50–100 times more viscous than the upper mantle (LM/UM). The predicted dynamic topography for a viscosity contrast of 50 between lithosphere and lower mantle best fits the amplitude of the total subsidence curve shown in Fig. 4, while not significantly degrading the fits to the global geoid. It is evident that while there is dynamic subsidence, the depocenter is located too far to the west with respect to the total subsidence curve, clearly reflecting the importance of including the full slab morphology in the dynamical calculations. To test the effects of the full slab geometry and buoyancy below the Pampas, we constructed a model for the slab under South America based on the morphology of Gutscher et al. (2000), with a slab dip of 30° E at the leading edge of the flat subduction (Fig. 3). The density contrasts of the slab (with respect to the surrounding mantle) account for seafloor age variations during subduction and thickening in the flat slab segment. Ages of subducted material were derived from the seafloor age reconstructions of Müller et al. (2008) and density contrasts for the flat-slab segment from Cembrano et al. (2006).

4. Results

4.1. Gravity anomalies

Bouguer gravity anomalies show an inverse correlation with elevation (Fig. 5), suggesting an isostatic compensation in the Sierras de Cordoba region. The gravity profile reproduces the lithospheric flexural results (see below). A broad-wavelength (~200 km wide) gravity “high” corresponds to the Pampean Plain (Fig. 5), with the lesser negative values across the San Guillermo High, where the

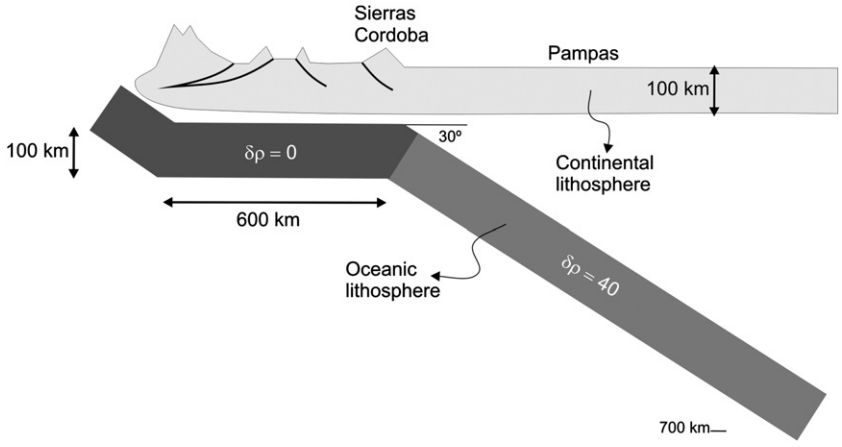

Fig. 3. Subduction geometry used in the dynamic topography instantaneous viscous flow model, showing the mantle and lithosphere structure. Notice the lateral density contrast variation and a flat-slab dipping of 30° at the leading edge. The kinematics analysis of subduction is based on Lithgow-Bertelloni and Richards (1998).

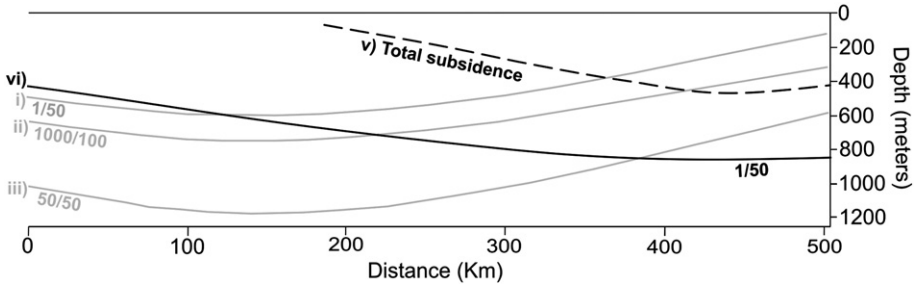

Fig. 4. Dynamic subsidence curves using vertical subduction from the trench (cf. Ricard et al., 1993) using different viscosity contrast relationships between lithosphere and lower mantle, 1000/100, 50/50 and 1/50. Notice that the 1/50 contrast better explains in amplitude the basin geometry. The curve ii simulates a flat slab with variations in the density contrast between the slab and mantle (see Appendix A and Fig. 3).

forebulge was interpreted from flexural analyses. Chase et al. (2009) have recently found a geoid high coincident with a flexural forebulge. However, the presence of the bulge is heavily dependent on the bandpass filter used on the observed geoid (Husson, personal communication). In the Bolivian–Brazilian foreland, Ussami et al. (1999) suggested an analogous gravity high, which correlates with the forebulge location at those latitudes. Shorter wavelength anomalies (10–50 km width, profile in Fig. 5) are likely influenced

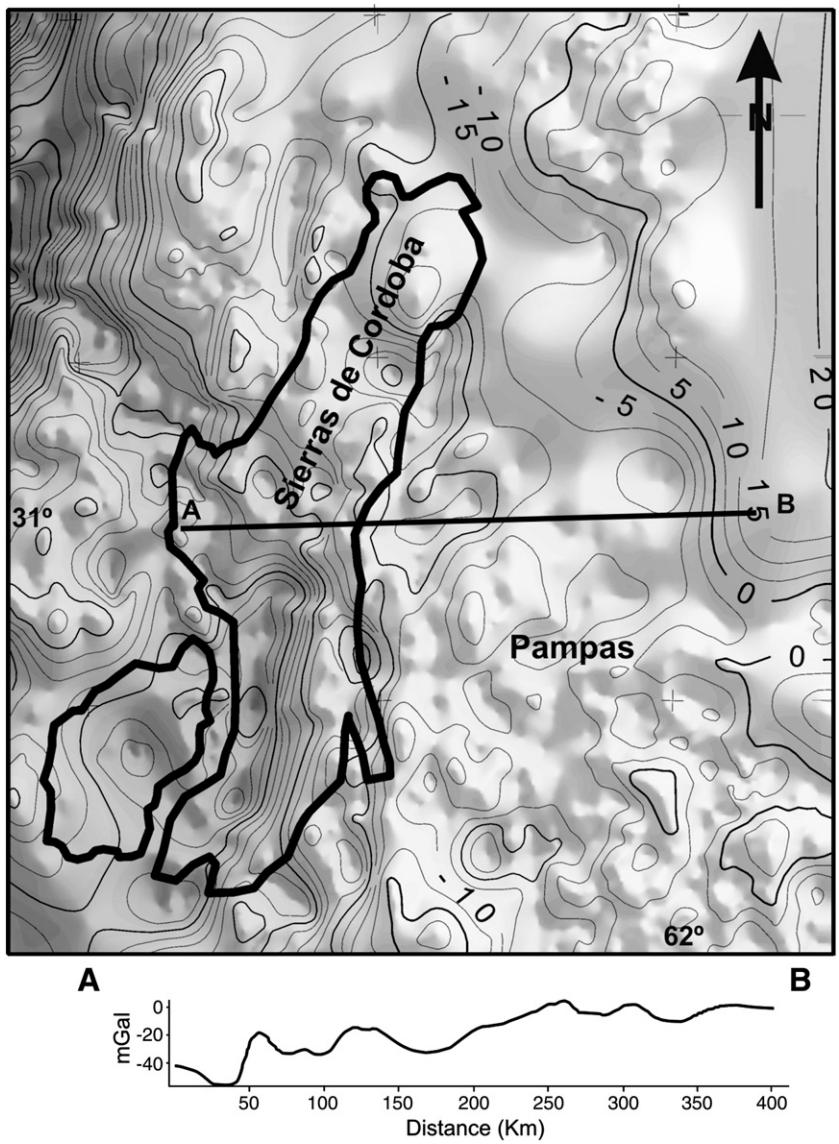

Fig. 5. Bouguer anomaly map and profile between the Sierras Cordoba and the Pampas. Grays in the map are positive mGals. Notice the less negative and positive values locate cratonward (to the east). The black arrow in the profile shows the location of the observed morphostructural bulge.

by the complex structure of the substrate of the basin, affected by Cretaceous normal faulting reworked by slight inversion during the Cenozoic.

4.2. Flexural analysis

The first flexural model (F1) reproduced a foredeep (distance from the tectonic load to the forebulge) width of ~250 km, a maximum accommodation amplitude of ~200 m close to the load, and a peripheral bulge amplitude of ~25 m (Fig. 2). These magnitudes match remarkably well with the modern morphotectonic regions of the Pampean Plain previously described, not only in wavelength and amplitude but also in the expected depositional systems (megafans from the load to the bulge and wetlands in the backbulge, to the east). This scenario suggests the Sierras de Cordoba loading reproduces the modern position of the Pampean depressions (foredeep and backbulge) and the location of the San Guillermo High (forebulge). However, F1 does not properly account for the preserved distribution and amount of Miocene–Present deposits, which are locally >400 m thick and ~300 km eastward with respect to the main load (Figs. 1B, 6).

Although F1 supposes the entire modern topography is Tertiary (maximum exhumation model), there is no Andean age thermochronological data in the Sierras de Cordoba. At the base of the highest relief (~3000 msl), the youngest apatite fission track (AFT) age is ca. 115–111 Ma (Early Cretaceous, Jordan et al., 1989). Assuming constant exhumation, paleogradients of ~17 °C/km (Collo and Dávila, 2008) and an AFT closure temperature of 90 °C–120 °C, the total exhumation since the Cretaceous would have been 5–7 km and the mean exhumation rate of 44–62 m/my. Considering that the most recent uplift in the Sierras de Cordoba affected ~7 Ma volcanic bodies (Pocho volcanoes, Kay and Gordillo, 1994), the Late Miocene–Pliocene exhumation would instead range between 308 and 434 m. Thus, we consider a second model (F2), which corresponds to a minimum exhumation scenario, with a load of 100 km (the orogen width) times 308 m or 434 m (the vertical uplift estimates, Fig. 2). The flexural wavelength is similar to F1 (~250 km), however, the maximum bending in the foredeep region close to the load is 119 and 143 m and the bulge amplitude 5 and 7 m, respectively (Fig. 2), much smaller than in F1. With this more realistic exhumation scenario it is even more difficult to explain the preserved strata shown in Fig. 6.

4.3. Dynamic topography

Fig. 6 shows the predicted dynamic topography in the Pampean Plain (subsidence wavelength ~500 km and subsidence amplitudes between ~−600 and −800 m). When the lower mantle is much more viscous than lithosphere (L/LM = 1/50), the dynamic topographic amplitude (−580.2 m) approximates to the sedimentary record amplitude (Fig. 6). Mantle-driven forces can generate, without the assistance of any other force or load, the accommodation spaces recorded in the Pampean foreland. However, when vertical subduction is considered (Fig. 6i), the predicted dynamic subsidence shows a horizontal offset (~400 km) with respect to the total subsidence curve (Fig. 6iv). More remarkably, however, is that when the full geometry of the flat slab segment is considered and the appropriate lateral variation in density contrasts between the flat slab segment and the normally dipping slab are considered, we reproduce the depocenter location almost exactly (compare curves ii and iv in Fig. 6). However, the predicted amplitudes are still larger than observed.

5. Discussion and conclusions

Flexural analyses and gravity studies indicate the Cenozoic uplift and loading of the Sierras de Cordoba can reproduce the regional morphostructure of the Pampean Plain (modern foreland), as evidenced by the good match between the flexural curves and the elevation models (Fig. 2). Yet, the Pampean basin is located behind the west vergent, crystalline-basement thrust sheets (Figs. 1B and 2), in opposite position with respect to the shift in deformation and loads. Supracrustal loading yields flexural curves mirrored with respect to the subsidence profiles so that the Pampean foreland might represent a case of depozones developed in opposed position with respect to the tectonic load migration. The influence of the Sierras de Cordoba topography on the Pampean flexure is also evident when accounting for the presence of the San Guillermo High (forebulge) along strike. The spatial development of the forebulge matches the highest altitudes of the Sierras de Cordoba (between 31° and 33° South latitude, see Fig. 2). Normal faults (Brunetto, 2008) on both sides of the San Guillermo forebulge (Fig. 2) are in favor of a flexural origin for this high, which can be reconciled in a bending-driven stretching setting (see Dávila et al., 2007).

The Mar Chiquita depression, located in the most distal foredeep (see Fig. 1), can be interpreted as a terminal alluvial belt dammed by the topographic closure of the San Guillermo forebulge. This indicates the modern Pampean foredeep is a modern case of an underfilled foreland basin dominated by megafan sedimentation. Basin starvation has been also proposed by numerical calculations (Pelletier, 2007). The occurrence of extended lagoons to the east of the forebulge (Fig. 1) reinforces a backbulge depozone interpretation for the areas located eastward of the San Guillermo High.

However, and more remarkably, although the flexural models reproduced the modern foreland morphostructure, they do not account for the subsurface sedimentary record (in magnitude and distribution, see Fig. 6). In fact, the curious geometry (Figs. 1B and 6iv) of the sedimentary record with the deepest preserved record to the east, suggests a likely erosion of the proximal depocenters close to the easternmost side of the Sierras de Cordoba during the basement-thrusting shift and previous to Pleistocene loess accumulation. This is in stark contrast to most foredeep depocenters, where the maximum subsidence occurs close to the loading (i.e. next to the topographic

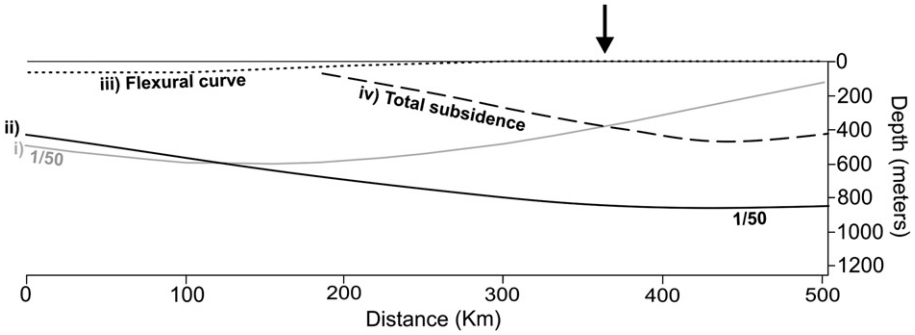

Fig. 6. Dynamic subsidence with a viscosity contrast between lithosphere and lower mantle = 1/50 (best fit) simulating a flat slab, with variations in the density contrast between the slab and mantle (see Appendix A and Fig. 3) and a slab leading edge dipping 30° eastward. Flexural (ii) and total subsidence (iii) curves are shown as reference. The black arrow shows the position of the forebulge.

highs). Independent of the incompleteness of the stratigraphic record close to the tectonic loads, the preserved basin profile is significantly offset with respect to the flexural calculations. The most conservative explanation is to think that the late Tertiary accommodation spaces (amplitudes) were, in part, inherited from earlier subsidence stages (early Tertiary or Mesozoic) or accommodated by compaction. On the basis of industry borehole data (Chebli et al., 1999), we discarded compaction of underlying strata as a subsidence mechanism (Fig. 7). The post-filling accommodation generated during burial of the Miocene–Modern successions (Fig. 7) is almost imperceptible. Because the middle Miocene marine strata were bent during the forebulge upwarping, locally capped by ~99 kyr loess beds (Brunetto, 2008), the loading and major subsidence episodes should postdate the Miocene marine incursion of central Argentina. Thus, the forebulge would have been uplifted during the Late Miocene–Pleistocene sedimentation break.

Therefore, it is likely that two different geodynamic processes are competing at different wavelengths (Fig. 8). While topographic loading explains the Pampas morphotectonics, the longer wavelength, expressed by the basin preservation, may be clearly driven by the dynamics of flat subduction as shown by Fig. 6. Non-isostatic loads, induced by slab sinking, trigger a significant negative dynamic topography in the pericratonic foreland and in the Pampean plain. Our mantle flow models demonstrate the best fit occurs when accurate geometry and density fields are incorporated in the calculations. The stress field generated by the sinking of slab material into the upper and lower mantle has an enormous contribution to Earth's surface topography. In fact, Pardo et al. (2002) demonstrated the presence of a remarkable vertical stress component in this region between 100 and 200 km depth, which might have been driven by mantle forces.

However, cumulative values of dynamic subsidence plus flexural tectonic subsidence are still much higher than the preserved stratigraphic thicknesses (total subsidence curve). Moreover, mantle dynamic modeling suggests overcompensation from the loads to the Pampean Plain, between ~0.8 and 0.5 km, which is in conflict with the gravity analyses. But our gravity and geoid/topography models are simple. The gravity model assumed a normal crust but the Pampas basement is a combination of two contrasting Protorezoic/Paleozoic terranes (Favetto et al., 2008), strongly affected by the Atlantic opening. The geoid, in turn, at degrees greater than 10 (wavelengths ~4000 km) is influenced by loads much shallower than those used here (Ricard et al., 2006). Lateral variations in viscosity, not included by the flow models, can localize subsidence sharply (Billen and Gurnis, 2001). Likewise, the location of density anomalies within the mantle and the lateral and radial density contrasts with the asthenosphere is likely more complex than we assumed here. More sophisticated studies of mantle flow, coupled with geophysical studies of the subsurface in this region, will allow us to solve these uncertainties and constrain the coupling between lithospheric deformation and mantle processes in an active orogen, which may also provide insight into orogenies influenced by flat-slab subduction such as the Laramide.

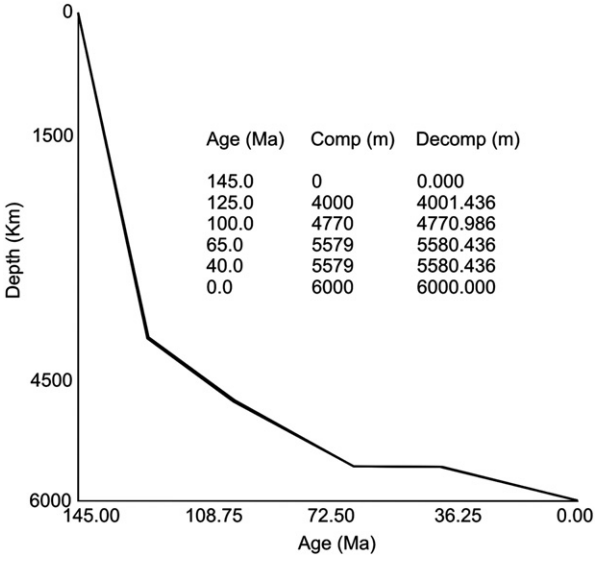

Fig. 7. Decompaction analysis (using OSXBackstrip by Cardozo, N.) that performs a 1D Airy backstripping with exponential reduction of porosity (Allen and Allen, 1990). Note the compacted and decompacted curves are imperceptible and overlapped, suggesting no accommodation by compaction of older units during the subsidence history. Stratigraphic and sedimentological data were supplied from a >5000-m depth oil borehole (see Webster et al. 2004 for details). Petrophysical properties (porosity and grain densities) were taken from Allen and Allen (1990).

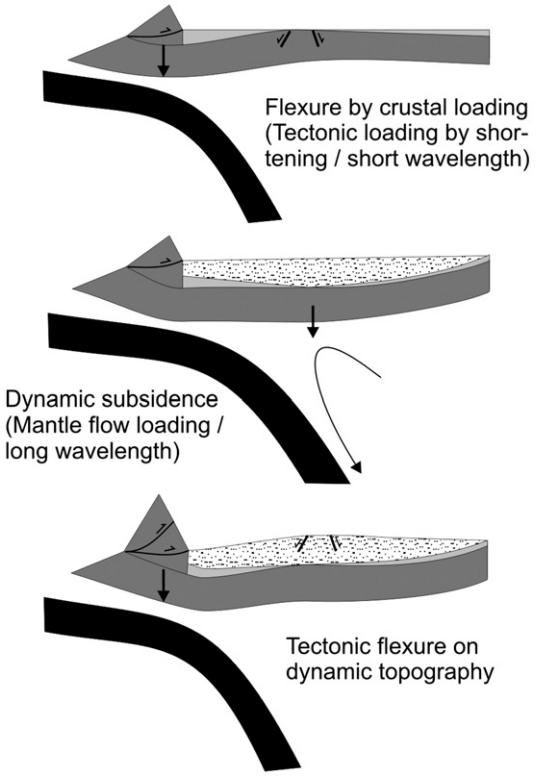

Fig. 8. Tectonic and geodynamic model showing the mechanisms competing at different wavelengths in the Argentine Pampas. While the shorter wavelengths are related to shortening and tectonics, the larger wavelength is connected to mantle-driven dynamics (dynamic topography).

Acknowledgements

Fulbright Commission, the Royal Society, CONICET, FONCyT and SECyT-UNC granted funds to FMD; CLB thanks NSF-EAR 0609553 and the Royal Society Incoming International Short Visit Fellowship. We thank an anonymous reviewer, L. Husson and B. Horton for substantive comments, which improved the clarity and impact of the manuscript.

Appendix A. Supplementary data

Supplementary data associated with this article can be found, in the online version, at doi:10.1016/j.epsl.2010.03.039.

References

Allen, P.A., Allen, J.R., 1990. Basin Analysis, Principles and Applications. Blackwell Scientific Publications.

Billen, M.I., Gurnis, M., 2001. A low viscosity wedge in subduction zones. Earth Planet. Sci. Lett. 193, 227–236.

Booker, J., Favetto, A., Pomposiello, C., 2004. Low electrical resistivity associated with plunging of the Nazca flat slab beneath Argentina. Nature 429, 399–403.

Brooks, B.A., Bevis, M., Smalley Jr., R., Kendrick, E., Manceda, R., Lauría, E., Maturana, R., Araujo, M., 2003. Crustal motion in the Southern Andes (26-36S): do the Andes behave like a microplate? Geochem. Geophys. Geosyst. 4 (10), 1085. doi:10.1029/2003GC000505.

Brunetto, E., 2008. Actividad neotectónica en el sector oriental de la cuenca inferior del Río Dulce, Laguna de Mar Chiquita y Bloque de San Guillermo. Unpublished PhD thesis, Universidad Nacional de Córdoba, Argentina, 271 pp.

Cardozo, N., Jordan, T.E., 2001. Causes of spatially variable tectonic subsidence in the Miocene Bermejo foreland basin, Argentina. Basin Res. 13, 335–357.

Cembrano, J., Lavenu, A., Yañez, G., Riquelme, R., Garcia, M., Gonzalez, G., Herail, G., 2006. Neotectonics. In: Gibbons, W., Moreno, T. (Eds.), The Geology of Chile. The Geological Society, pp. 231–262.

Chase, C.G., Sussman, A.J., Coblentz, D.D., 2009. Curved Andes: geoid, forebulge, and flexure. LIthosphere 1 (6), 358–363.

Chebli, G.A., Mozetic, M.E., Rossello, E.A., Buhler, M., 1999. Cuencas sedimentarias de la Llanura Chacopampeana. In: Caminos, R. (Ed.), Geología Argentina. : Anales, 29. Instituto de Geología y Recursos Minerales, Buenos Aires, pp. 627–644.

Collo, G., Dávila, F.M., 2008. Burial history and estimation of ancient thermal gradients in deep synorogenic foreland sequences: an approach in the Neogene Vinchina basin, south-Central Andes. 7th ISAG 2008, Nice, France.

Dávila, F.M., Astini, R.A., Jordan, T.E., Gehrels, G., Ezpeleta, M., 2007. Miocene forebulge development previous to the broken foreland partitioning in the southern Central Andes, west-central Argentina. Tectonics 26, TC5016. doi:10.1029/2007TC002118.

DeCelles, P.G., Giles, K.A., 1996. Foreland basin systems. Basin Res. 8, 105–123.

Favetto, A., Pomposiello, C., Lopez de Luchi, M.G., Booker, J., 2008. 2D magnetotelluric interpretation of the crust electrical resistivity across the Pampean terrane–Rio de la Plata suture, in central Argentina. Tectonophysics 459, 54–65.

Garcia-Castellanos, D., Fernandez, M., Torne, M., 2002. Modeling the evolution of the Guadalquivir foreland basin (southern Spain). Tectonics 21. doi:10.1029/2001TC001339.

Gurnis, M., 1990. Ridge spreading, subduction, and sea level fluctuations. Science 250, 970–972.

Gutscher, M.-A., Spakman, W., Bijwaard, H., Engdahl, E.R., 2000. Geodynamics of flat subduction; seismicity and tomographic constrains from the Andean margin. Tectonics 19, 814–833.

Hager, B.H., O'Connell, R.J., 1981. A simple model of plate dynamics and mantle convection. J. Geophys. Res. 86, 4843–4867.

Hernández, R., Jordan, T., Dalentz Farjat, A., Echavarría, L., Idleman, B., Reynolds, J., 2005. Age, distribution, tectonics and eustatic controls of the Paranense and Caribbean marine transgressions in southern Bolivia and Argentina. J. S. Am. Earth Sci. 19, 495–512.

Hinze, W., 2003. Bouguer reduction density, why 2.67. Geophysics 68, 1559–1560.

Hinze, W., et al., 2005. New standards for reducing gravity data: the North American gravity database. Geophysiscs 70, J25–J32.

Horton, B.K., DeCelles, P.G., 1997. The modern foreland basin system adjacent to the Central Andes. Geology 25, 895–898.

Jordan, T.E., Allmendinger, R.W., 1986. The Sierras Pampeanas of Argentina: a modern analogue of Rocky Mountain foreland deformation. Am. J. Sci. 286, 737–764.

Jordan, T.E., Zeitler, P., Ramos, V.A., Gleadow, A.J.W., 1989. Thermocronometric data on the development of the basement peneplain in the Sierras Pampeanas, Argentina. J. S. Am. Earth Sci. 2, 207–222.

Jordan, T.E., Allmendinger, R.W., Damanti, J.F., Drake, R.E., 1993. Chronology of motion in a complete thrust belt: the Precordillera, 30–31°S, Andes Mountains. J. Geol. 101, 135–156.

Kane, M.F., 1962. A comprehensive system of terrain corrections using a digital computer. Geophysics 27, 455–462.

Kay, S.M., Gordillo, C.E., 1994. Pocho volcanic rocks and the melting of depleted continental lithosphere above a shallowly dipping subduction zone in the central Andes. Contrib. Mineralog. Petrol. 117, 25–44.

Kay, S.M., Mpodozis, C., 2002. Magmatism as a probe to the Neogene shallowing of the Nazca plate beneath the modern Chilean flat-slab. J. S. Am. Earth Sci. 15, 39–57.

Lithgow-Bertelloni, C., Richards, M.A., 1998. The dynamic of Mesozoic and Cenozoic plate motion. Rev. Geophys. 36, 27–78.

Liu, S., Nummedal, D., 2004. Late Cretaceous subsidence in Wyoming: quantifying the dynamic component. Geology 32, 397–400.

Liu, L., Spasojevic, S., Gurnis, M., 2008. Reconstructing Farallon Plate Subduction beneath North America back to the Late Cretaceous. Science 322, 934–938.

Marengo, H.G., 2006. Micropaleontología y estratigrafía del Mioceno marino de la Argentina: Las Transgresiones de Laguna Paiva y del "Entrerriense-Paranense", Tomo 1. Unpublished PhD Thesis, Universidad de Buenos Aires, Argentina, 124 pp.

Mitrovica, J.X., Beaumont, C., Jarvis, G.T., 1989. Tilting of the continental interior by the dynamical effects of subduction. Tectonics 8, 1079–1094.

Müller, R.D., Sdrolias, M., Gaina, C., Roest, W.R., 2008. Age, spreading rates, and spreading asymmetry of the world's ocean crust. Geochem. Geophys. Geosyst. 9, Q04006. doi:10.1029/2007GC001743.

Nagy, D., 1966. The gravitational attraction of a right rectangular prism. Geophysics 31, 362–371.

Pardo, M., Comte, D., Monfret, T., 2002. Seismotectonic and stress distribution in the central Chile subduction zone. J. South Am. Earth Sci. 15, 11–22.

Pelletier, J.D., 2007. Erosion-rate determination from foreland basin geometry. Geology 35, 5–8.

Pérez-Gussinyé, M., Lowry, A.R., Watts, A.B., 2007. Effective elastic thickness of South America and its implications for intracontinental deformation. Geochem. Geophys. Geosys. 8 (5), 1–22. doi:10.1029/2006GC001511.

Pysklywec, R.N., Mitrovica, J.X., 1999. The role of subduction-induced subsidence in the evolution of the Karoo Basin. J. Geol. 107, 155–164.

Ramos, V.A., 2008. The basement of the Central Andes: the Arequipa and related terranes. Ann. Rev. Earth Planet. Sci. 36, 289–324.

Ricard, Y., Richards, M., Lithgow-Bertelloni, C., LeStunff, Y., 1993. A geodynamical model of mantle density heterogeneity. J. Geophys. Res. 98, 21895–21909.

Ricard, Y., Chambat, F., Lithgow-Bertelloni, C., 2006. Gravity observations and 3D structure of the Earth (Comptes Rendus de l'Acad (c)mie des Sciences) C. R. Geosci. 338, 992–1001.

Tassara, A., 2005. Interaction between the Nazca and South American plates and formation of the Altiplano–Puna plateau: review of a flexural analysis along the Andean margin (15°–34°S). Tectonophysics 399, 39–57.

Tassara, A., Swain, C., Hackney, R., Kirby, J., 2007. Elastic thickness structure of South America estimated using wavelets and satellite-derived gravity data. Earth Planet. Sci. Lett. 253, 17–36.

Turcotte, D.L., Schubert, G., 2002. Geodynamics, 2nd ed. Cambridge University Press.

Ussami, N., Shiraiwa, S., Landim Dominguez, J.M., 1999. Basement reactivation in a Plio–Pleistocene Sub-Andean foreland flexural bulge: the Pantanal Wetland, SW Brazil. Tectonics 18, 25–39.

Webster, R., Chebli, G.A., Fischer, J.F., 2004. General Levalle Basin, Argentina; a frontier Lower Cretaceous rift basin. AAPG Bull. 88 (5), 627–652.